REFERENCES AND NOTES

1. K. S. Chester, *Q. Rev. Biol.* **8**, 275 (1933); J. Kúc, *BioScience* **32**, 854 (1982); A. F. Ross, *Virology* **14**, 340 (1961); in *Viruses of Plants*, A. B. R. Beemster and J. Dijkstra, Eds. (North-Holland, Amsterdam, 1966), p. 127; S. Gianinazzi, in *Plant Microbe Interactions: Molecular and Genetic Perspectives*, E. W. Nester and T. Kosuge, Eds. (Macmillan, New York, 1984), vol. 1, p. 321.
2. J. P. Métraux *et al.*, in *Molecular Genetics of Plant-Microbe Interactions*, H. Hennecke and D. P. Verma, Eds. (Kluwer, Dordrecht, Netherlands, 1991), vol. 1, p. 432.
3. L. C. Van Loon and J. Antoniw, *Neth. J. Plant Pathol.* **88**, 237 (1982).
4. E. Ward *et al.*, *Plant Cell* **3**, 1085 (1991).
5. S. Uknes *et al.*, *ibid.* **4**, 645 (1992); J. P. Métraux *et al.*, *Proc. Natl. Acad. Sci. U.S.A.* **86**, 896 (1989).
6. F. Mauch *et al.*, *Plant Physiol.* **88**, 936 (1988); W. K. Roberts and C. P. Selitrennikoff, *J. Gen. Microbiol.* **134**, 169 (1988); *ibid.* **136**, 1771 (1990); A. J. Vigers, W. K. Roberts, C. P. Selitrennikoff, *Mol. Plant Microbe Interactions* **4**, 315 (1991); C. P. Woloshuk *et al.*, *Plant Cell* **3**, 619 (1991).
7. D. Alexander *et al.*, *Proc. Natl. Acad. Sci. U.S.A.*, in press.
8. J. Malamy, J. P. Carr, D. F. Klessig, I. Raskin, *Science* **250**, 1002 (1990).
9. J. P. Métraux *et al.*, *ibid.*, p. 1004.
10. R. F. White, *Virology* **99**, 410 (1979).
11. S. Yamamoto, M. Katagiri, H. Maeno, O. Hayaishi, *J. Biol. Chem.* **240**, 3408 (1965).
12. K.-M. Yen and I. C. Gunsalus, *Proc. Natl. Acad. Sci. U.S.A.* **79**, 874 (1982); I.-S. You, D. Ghosal, I. C. Gunsalus, *Biochemistry* **30**, 1635 (1991).
13. The 1.5-kb Ssp I to Hpa I fragment from plasmid pSR20 (a subclone of NAH7) was ligated to Eco RI linkers, digested with Eco RI, and subcloned into pCGN1761 [L. Comai, P. Moran, D. Maslyar, *Plant Mol. Biol.* **15**, 373 (1990)] behind an enhanced 35S promoter from cauliflower mosaic virus [K. McBride and K. Summerfelt, *ibid.* **14**, 269 (1990)]. We digested the resulting plasmid with Xba I to release a 4.8-kb fragment containing the promoter, the *nahG* coding sequence, and a *tml* 3′ terminator sequence. The Xba I fragment was ligated into the binary vector pCIB200 and the resulting plasmid was transformed into *Agrobacterium tumefaciens* CIB542 [S. Uknes *et al.*, *Plant Cell* **5**, 159 (1993)]. *Nicotiana tabacum* cv. xanthi.nc leaf disks were transformed essentially as described [R. B. Horsch *et al.*, *Science* **227**, 1229 (1985)] with the *Agrobacterium* strain containing the *nahG* construct.
14. *Nicotiana tabacum* cv. xanthi.nc and transgenic *nahG* tobacco plants were inoculated with TMV or mock-inoculated with buffer and carborundum as described [G. Payne *et al.*, *Proc. Natl. Acad. Sci. U.S.A.* **87**, 98 (1990)]. We treated a total of eight plants of each line. Tissue from mock-inoculated (*19*) or TMV-inoculated plants was harvested and pooled 7 days after inoculation. We extracted RNA as described [M. Lagrimini, W. Burkhart, M. Moyer, S. Rothstein, *ibid.* **84**, 7542 (1987)] and analyzed it by RNA blot hybridization [F. Ausubel *et al.*, *Current Protocols in Molecular Biology*, (Wiley, New York, 1987)]. We probed the gel blots with a ^{32}P-labeled DNA fragment containing the *nahG* coding sequence. Seven days after infection secondary, uninfected leaves were inoculated with TMV. Leaves were photographed 6 days after this inoculation.
15. We lyophilized and extracted the harvested tissue with sample buffer (125 mM tris, 10% β-mercaptoethanol, 4% SDS, 20% glycerol, 0.002% bromophenol blue) using 45 mg of tissue per milliliter of buffer. The protein extracts were separated by SDS–polyacrylamide gel electrophoresis on a 10 to 20% tris-tricine gel (Novex). The polypeptides were then electroblotted [H. Towbin, T. Staehlin, J. Gordon, *Proc. Natl. Acad. Sci. U.S.A.* **76**, 4350 (1979)] to nitrocellulose and immunostained as described [L. H. Pratt, D. W. McCurdy, Y. Shimazaki, M. M. Cordonnier, *Mod. Methods Plant Anal. New Ser.* **4**, 51 (1986)]. Antiserum was prepared by Berkeley Antibody Company (San Francisco) from rabbits injected with salicylate hydroxylase isolated from *Escherichia coli* containing the *nahG* coding sequence in the pGEX-2T expression plasmid (Pharmacia LKB Biotechnology).
16. Salicylic acid was extracted from leaf tissue essentially as described (*17*), except the samples were not allowed to overdry, and the final dried samples were resuspended in 500 μl of 20% methanol. We injected 10 to 100 μl of this suspension onto a Dynamax 60A, 8-μm, C-18 (4.6 mm by 25 cm) column with a guard column (Rainin Instruments, Emeryville, CA) maintained at 40°C. Isocratic separation was performed at 1 ml/min using 20% (v/v) methanol in 20 mM sodium acetate, pH 5.0. Fluorescence detection was done with a Model 980 detector (ABI/Kratos Analytical, Foster City, CA) with a 5 μl flow cell, deuterium lamp with a 295-nm excitation setting, and a 370-nm cutoff emission filter. The limit of detection was 500 pg of SA in 50 μl. Quantitation was determined versus a linear range (10 to 1000 ng/ml) of calibration standards for sodium salicylate.
17. N. Yalpani *et al.*, *Plant Cell* **3**, 809 (1991).
18. J. Malamy, J. Hennig, D. Klessig, *ibid.* **4**, 359 (1992).
19. T. Gaffney *et al.*, unpublished data.
20. S. C. El-Basyouni *et al.*, *Phytochemistry* **3**, 485 (1964).
21. B. Marshall and C. Ratledge, *Biochim. Biophys. Acta* **264**, 106 (1972).
22. J. Rasmussen, R. Hammerschmidt, M. Zook, *Plant Physiol.* **97**, 1342 (1991).

23. We thank S. Dincher for initial experiments showing that catechol was not an inducer of SAR; S. Dincher, G. Crawford, S. Sips, and P. VanBourgondien for horticultural support; D. Maddox for assistance on the statistical analysis; M. Schell for providing pSR20; M.-D. Chilton, B. Miflin, B. Lee, T. Brears, D. Alexander, T. Delaney, S. Foley, and K. Lawton for critically reading the manuscript; and B. Gibbons, F. Beard, and D. Hill for providing T.G. with the necessary inspiration to apply *Pseudomonas* genetics toward a better understanding of SAR.

9 April 1993; accepted 4 June 1993

Dialkylglycine Decarboxylase Structure: Bifunctional Active Site and Alkali Metal Sites

Michael D. Toney,* Erhard Hohenester, Sandra W. Cowan,† Johan N. Jansonius‡

The structure of the bifunctional, pyridoxal phosphate–dependent enzyme dialkylglycine decarboxylase was determined to 2.1–angstrom resolution. Model building suggests that a single cleavage site catalyzes both decarboxylation and transamination by maximizing stereoelectronic advantages and providing electrostatic and general base catalysis. The enzyme contains two binding sites for alkali metal ions. One is located near the active site and accounts for the dependence of activity on potassium ions. The other is located at the carboxyl terminus of an α helix. These sites help show how proteins can specifically bind alkali metals and how these ions can exert functional effects.

Pyridoxal-5′-phosphate (PLP) is the most versatile of all the known coenzymes. Its preponderance in amino acid metabolism arises from its ability to labilize all four bonds to the α carbon and, less commonly, those to the β and γ carbons. The broad-ranging power of PLP is explained by the general mechanism proposed by Metzler *et al.* and Braunstein and Shemyakin (*1*), which invokes a central, carbanionic quinonoid intermediate.

Dialkylglycine decarboxylase (DGD) from *Pseudomonas cepacia* is an unusual PLP-dependent enzyme that catalyzes both decarboxylation and transamination in its normal catalytic cycle (*2*). In the first half-reaction, dialkylglycines such as α-methylalanine are oxidatively decarboxylated to give CO_2 and a ketone, with amino group transfer to the coenzyme. The second half-reaction is a classical transamination with pyruvate as substrate. This intriguing ability to catalyze rapidly both decarboxylation and transamination provided the impetus for the present study.

The DGD is a tetramer, built up as a dimer of dimers (Fig. 1 and Tables 1 and 2) (*3*). The fold of DGD is related to those of aspartate aminotransferase (AAT) (*4*), ω-amino acid aminotransferase (*5*), and tyrosine phenol-lyase (*6*) and likely represents a general template for a large family of PLP-dependent enzymes. Each DGD monomer is composed of two distinct domains and an NH_2-terminal segment. The large domain contains the PLP binding site and consists of a central, seven-stranded β sheet surrounded by eight α helices in a typical αβ fold. The small domain comprises a four-stranded β sheet with three α helices packed against the face opposite the large domain. The NH_2-terminal helix is spatially removed from the bulk of the subunit and forms a clamp to the neighboring subunit. A small, three-stranded β sheet completes the NH_2-terminal segment.

Department of Structural Biology, Biocenter of the University of Basel, Klingelbergstrasse 70, 4056 Basel, Switzerland.

*Present address: Department of Chemistry, University of California, Berkeley, CA 94720.
†Present address: Ciba-Geigy AG, Biotechnology, K-681.5.03, P.O. Box, 4002 Basel, Switzerland.
‡To whom correspondence should be addressed.

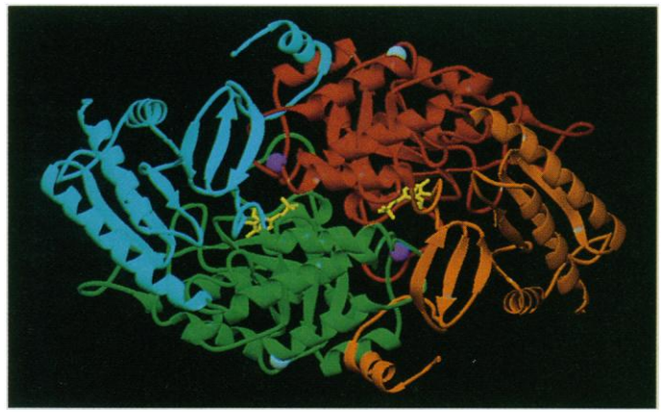

Fig. 1. Ribbon representation (*18*) of the DGD dimer. The view is directly down the dimer twofold symmetry axis. One subunit is green (large domain) and blue (small domain plus NH_2-terminal segment), whereas the other is red and gold. The PLP cofactors are yellow; K^+ ions, purple; and Na^+ ions, white.

Table 1. Structure determination by the isomorphous replacement method (*3*). Buffer B was used for all but the native A data set, for which buffer A was used. Res., resolution; Refl., reflections; Compl., completeness; and rms, root mean square.

Data set	Res. (Å)	Refl. (no.)	Compl. (%)	R_{merge}* (%)	ΔF† (%)	Sites‡	$R_{centric}$§ (%)	F_H/E‖
Native A	2.6	16,640	88	6.5	17.8			
Native B	2.1	32,665	93	7.8				
$TlCl_3$	3.1	5,634	50	7.7	14.9	1, 2	44	1.78
PPL-Cys-Hg	2.9	12,656	94	8.4	15.8	1, 2	45	1.71
EMTS	3.2	7,519	74	7.5	19.3	1–3	37	2.21
$KAu(CN)_2$	3.1	8,119	72	8.1	21.5	1–3	40	2.08
TlCl	2.7	15,745	92	8.3	23.7	1–4	40	2.04

*$R_{merge} = \Sigma|I - \langle I\rangle|/\Sigma I$. †$\Delta F = \Sigma|F_{deriv} - F_{native}|/\Sigma F_{native}$; with respect to native B. ‡The numbers correspond to the four heavy atom binding sites near Cys^{258}, Cys^{350}, Cys^{60}, and Cys^{386}. §$R_{centric} = \Sigma||F_{deriv} \pm F_{native}| - F_H(calc)|/\Sigma|F_{deriv} \pm F_{native}|$. ‖$F_H/E$ = "phasing power" = (rms calculated F_H)/(rms error).

Table 2. Refinement (*3*). Restrained isotropic *B* factors and free individual *B* factors were refined for native A and native B, respectively. The final models for native A and native B both contain a MES buffer molecule in the active site and two metal ions (native A: one K^+ and one Na^+; native B: two Na^+). The density in native B corresponding to residues 142 and 143, 346 and 347, and 369 to 377 is weak. The main chain torsion angles of all nonglycine residues lie within the allowed regions of the Ramachandran plot. Bond lengths and angles and planar group measurements are root-mean-square (rms) deviations from the target values.

Model	Res. (Å)	Compl.* (atoms)	Water (no.)	R_{factor}† (%)	Bond lengths (Å)	Bond angles (deg.)	Planar groups (Å)
Native A	8 to 2.6	3281	145	17.6	0.013	2.5	0.009
Native B	8 to 2.1	3048	229	17.8	0.011	2.2	0.008

*Out of a total of 3281 atoms. †$R_{factor} = \Sigma|F_{obs} - F_{calc}|/\Sigma F_{obs}$.

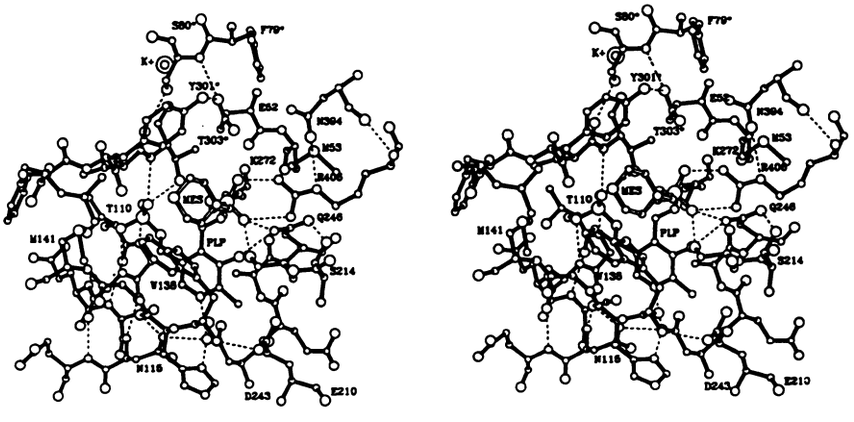

Fig. 2. Stereo view of the DGD active site. Located in the center of the figure, PLP is covalently bound to Lys^{272} through an imine linkage. A MES ion is located at the substrate binding site (open bonds). Asterisks denote residues contributed by the other subunit in the dimer. Water molecules have been omitted for clarity. Dashed lines indicate hydrogen bonds.

The active site (Fig. 2) is located near the monomer-monomer interface and is composed of residues from both subunits in the dimer. The PLP is tightly bound to the protein through several specific interactions, most notably the covalent Schiff base linkage to Lys^{272} and the hydrogen bond–salt bridge between Asp^{243} and the pyridine nitrogen. The latter interaction ensures a strong electron sink capable of stabilizing the obligatory carbanionic intermediates.

Dunathan (*7*) proposed a model for control of the reaction specificity of PLP-dependent enzymes: The scissile bond of the external aldimine intermediate must be oriented perpendicularly to the coenzyme π-bonding system to maximize σ-π orbital overlap in the transition state and, thereby, the reaction rate. Models of the L-isovaline and L-alanine external aldimine intermediates in DGD (*8*) suggest that this is true for both the decarboxylation and transamination half-reactions, as this orientation additionally provides for the necessary electrostatic and general base catalysis.

The L-isovaline carboxylate group, when oriented perpendicularly to the coenzyme ring plane, is in van der Waals contact with the Glu^{52} carboxylate group and may form hydrogen bonds with Lys^{272} and Arg^{406}. Thus, electrostatic destabilization by Glu^{52} of the negatively charged carboxylate likely plays a major role in the decarboxylation step. A similar mechanism has been proposed for pyruvate-dependent histidine decarboxylase (*9*). Decarboxylation rate enhancement by electrostatic destabilization has also been observed in relevant model reactions and catalytic antibodies (*10*).

Transamination would occur with the C_α–H bond of the L-alanine external aldimine oriented perpendicularly to the coenzyme ring plane. This half-reaction is likely general base catalyzed as is the transamination catalyzed by AAT, where Lys^{258} is the sole general base catalyst (*11*). Lys^{272} in DGD is positioned analogously to Lys^{258} in AAT (*4*) and presumably performs a similar mechanistic role.

Strong, spherical electron density at two positions in the partially refined models together with the presence of appropriately disposed oxygen ligands suggested the presence of two metal ions (Fig. 1), one near the active site (site 1) and the other on the surface of the protein (site 2). Calcium was excluded as a metal ion candidate for both

sites by the low Ca^{2+} content of our two samples, native A and B crystals (*12*). The native A model is assigned as K^+ at site 1 and Na^+ at site 2, whereas the native B model is assigned as Na^+ at both sites. These assignments are based on *B* factors and difference electron density maps (*13*), metal-ligand distances (*14*), the demonstrated dependence of DGD stability and activity on K^+ (*15*), and the metal ion content of the buffers (*3*).

Metal binding site 1 (Figs. 3 and 4) accounts for the dependence of DGD activity on K^+ ions (*15*). It appears that the bound ion is too distant from the reaction center (11 Å from the coenzyme aldimine nitrogen) to play a direct role in catalysis. The exchange of Na^+ for K^+ results in a gross change in the coordination geometry from octahedral to distorted trigonal bipyramidal with a concomitant reduction in the average metal-ligand distance from 2.73 ± 0.12 to 2.33 ± 0.16 Å. In addition to movements of the loops that make up the metal ion binding site, a concerted rearrangement of the conformations of Ser^{80} and Tyr^{301}, as well as small structural changes extending far beyond the immediate surroundings of the metal ion, are observed.

The structural consequences of the replacement of K^+ by Na^+ at site 1 provide a viable explanation for the strong inhibitory effects of Na^+ and Li^+ on DGD activity reported by Aaslestad *et al.* (*15*). The reorientations of Tyr^{301}, which likely interacts directly with bound substrate, and Ser^{80}, a K^+ ligand, in the active site disrupt the hydrogen bonding to the Glu^{52} carboxylate group, which is strongly implicated in the catalytic mechanism.

Metal binding site 2 (Fig. 4) is formed by oxygen ligands from a tight reverse turn at the COOH-terminus of the α helix that precedes the first strand of the central β sheet. The Na^+ ion fits snugly into the Pro-Pro-Gly-Leu turn created by residues 99 to 102, reminiscent of alkali metal ion binding to natural ionophores and synthetic macrocyclic ligands (*16*). The coordination geometry is octahedral, with an average metal-ligand distance of 2.42 ± 0.12 Å in native B. None of the ligands are contributed by a carboxylate group, unlike in all well-characterized Ca^{2+} sites, and charge compensation is presumably afforded by the helix macrodipole.

The enzyme DGD shares its catalytic requirement for monovalent cations with a large number of enzymes (*17*), and it is possible that this initial insight is merely a prelude to the structural characterization of a large class of biologically important ion binding sites.

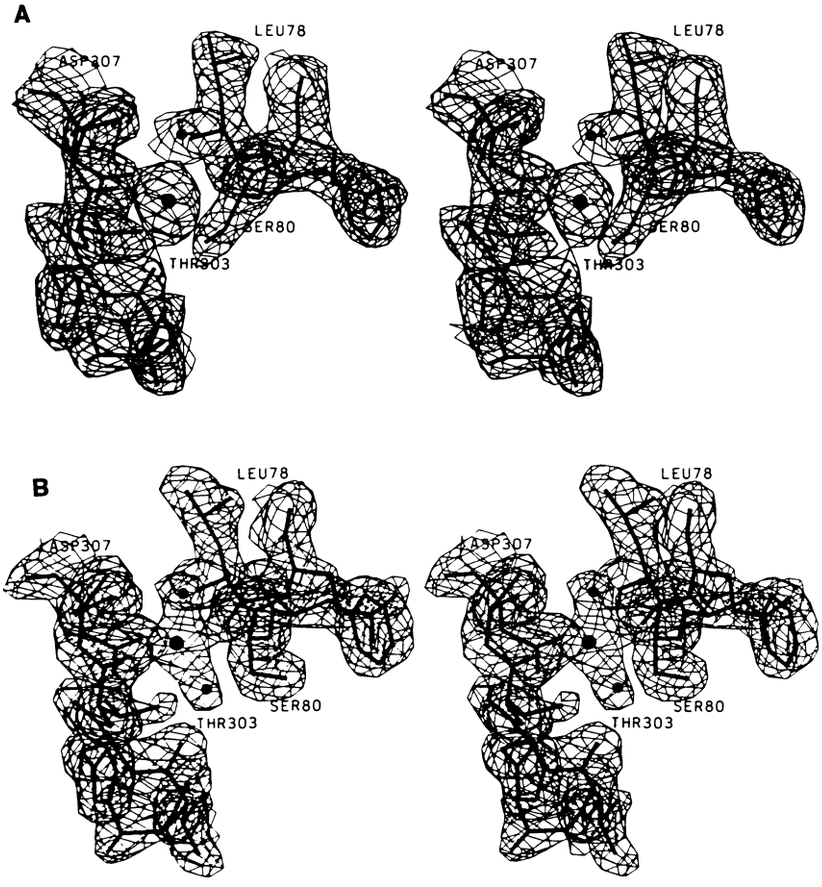

Fig. 3. Stereo pairs showing the refined ($2F_{obs} - F_{calc}$), α_{calc} electron density maps at alkali metal binding site 1. (**A**) Native A structure (2.6 Å resolution) with K^+ bound. (**B**) Native B structure (2.1 Å resolution) with Na^+ bound. The maps are contoured at the 1.5σ level. Metal ions and water molecules are shown as large and small black spheres, respectively.

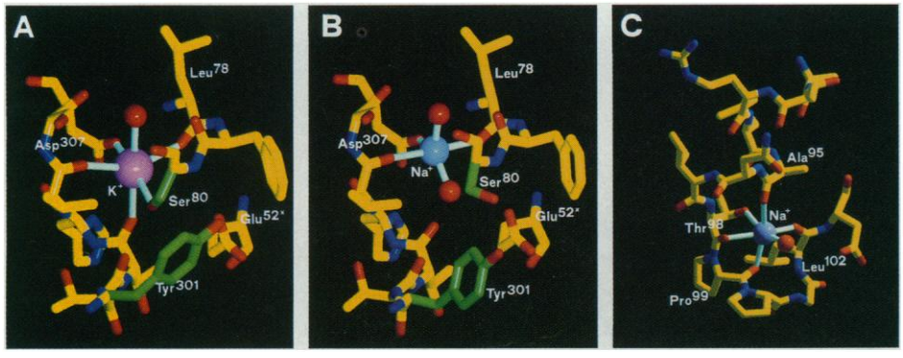

Fig. 4. Monovalent cation binding sites in DGD. (**A**) K^+ (native A) and (**B**) Na^+ (native B) bound at site 1, near the active site. The side chains of Ser^{80} and Tyr^{301} are in green to emphasize the conformational change accompanying the exchange of ions. (**C**) Na^+ site (site 2) near the surface of the protein. Water molecules are depicted as red spheres. Superscript x denotes residue contributed by the second subunit in the dimer.

REFERENCES AND NOTES

1. D. E. Metzler *et al.*, *J. Am. Chem. Soc.* **76**, 648 (1954); A. E. Braunstein and M. M. Shemyakin, *Biochemistry* (*Moscow*) **18**, 393 (1953).
2. G. B. Bailey and W. B. Dempsey, *Biochemistry* **6**, 1526 (1967); J. W. Keller *et al.*, *J. Biol. Chem.* **265**, 5531 (1990).
3. Crystals were grown as described by M. D. Toney *et al.* [*J. Mol. Biol.* **222**, 873 (1991)]. All data except native B were collected on an Enraf-Nonius FAST area detector and were processed using the program MADNES [A. Messerschmidt and J. W. Pflugrath, *J. Appl. Crystallogr.* **20**, 306 (1987)]. Native B data combine 2.1 Å image plate data {EMBL, Hamburg; processed using the program MOSFLM [A. G. W. Leslie, P. Brick, A. J. Wonacott, *CCP4 News* **18**, 33 (1986)] adapted for image plates} and FAST data from 15 to 3.6 Å. Native A data were collected from a crystal taken directly from the crystallization drop [buffer A: 15% PEG4000, 75 mM sodium pyruvate, 15 mM

2-(*N*-morpholino)-ethanesulfonic acid (MES)–KOH (pH 6.1), 15 μM PLP], whereas all other data were collected from crystals soaked in stabilization buffer [buffer B: 20% PEG4000, 100 mM sodium pyruvate, 30 mM MES-NaOH (pH 6.1), 20 μM PLP]. All derivatives were isomorphous only with the native B data. The major heavy atom binding sites were found with vector searches of difference Patterson maps by standard CCP4 programs [CCP4, *SERC U.K. Collaborative Computing Project No. 4* (Daresbury Laboratory, United Kingdom, 1979)]. Heavy atom parameters were refined against the centric data and multiple isomorphous replacement (MIR) phases were calculated. The 2.8 Å MIR map was improved with several cycles of solvent flattening [B.-C. Wang, *Methods Enzymol.* **115**, 90 (1985)]. A model containing 88% of the atoms was built with the program O [T. A. Jones and M. Kjelgaard, *Manual for O* (Uppsala University, Uppsala, Sweden, 1990)] into a map flattened at 45% solvent content and was refined with X-PLOR [A. T. Brünger, *X-PLOR Manual* (Yale Univ. Press, New Haven, CT, 1990)] and a simulated annealing protocol. Combination of MIR and partial model phases and additional solvent flattening resulted in a map that allowed the entire sequence to be traced. A second application of simulated annealing at 2.8 Å resolution was performed. The native A structure was obtained by direct refinement of the native B model against native A data with an X-PLOR simulated annealing protocol. Thereafter, refinement proceeded with the program TNT [D. E. Tronrud, L. F. Ten Eyck, B. W. Matthews, *Acta. Crystallogr. Sect. A* **43**, 489 (1987)] with all observed data between 8 Å and the respective high-resolution limits.

4. J. N. Jansonius and M. G. Vincent, in *Biological Macromolecules and Assemblies*, F. A. Jurnak and A. McPherson, Eds. (Wiley-Interscience, New York, 1987), vol. 3, pp. 187–286; C. A. McPhalen, M. G. Vincent, J. N. Jansonius, *J. Mol. Biol.* **225**, 495 (1992); G. C. Ford, G. Eichele, J. N. Jansonius, *Proc. Natl. Acad. Sci. U.S.A.* **77**, 2559 (1980).
5. N. Watanabe *et al.*, *J. Biochem.* (*Tokyo*) **105**, 1 (1989).
6. A. A. Antson *et al.*, *Biochemistry* **32**, 4195 (1993).
7. H. C. Dunathan, *Proc. Natl. Acad. Sci. U.S.A.* **55**, 712 (1966).
8. External aldimine models were built on minimal assumptions and manipulations of the enzyme structure. The coenzyme ring in the aldimine models is rotated forward (in the view of Fig. 2) compared with the holoenzyme to relieve steric clashes. By analogy to AAT (*4*), this rotation was achieved by a change in only the C4-C5-C5′-OP1 torsion angle of PLP (64° to 91°). The indole ring of Trp^{138} rotates to near planarity with the PLP ring to accommodate the change in coenzyme conformation.
9. T. Gallagher, E. E. Snell, M. L. Hackert, *J. Biol. Chem.* **264**, 12737 (1989).
10. M. H. O'Leary, *Acc. Chem. Res.* **21**, 450 (1988); J. F. Marlier and M. H. O'Leary, *J. Am. Chem. Soc.* **108**, 4896 (1986); J. A. Ashley *et al.*, *ibid.* **115**, 2515 (1993).
11. M. D. Toney and J. F. Kirsch, *Science* **243**, 1485 (1989); *Biochemistry* **32**, 1471 (1993).
12. DGD crystals were dissolved, the protein was hydrolyzed (10 M hydrochloric acid, 90°C, 1.5 hours), and the Ca^{2+} content was determined fluorometrically [J. P. Y. Kao, A. T. Harootunian, R. Y. Tsien, *J. Biol. Chem.* **264**, 8179 (1989)] to be less than 0.2 and 0.1 Ca^{2+} per DGD monomer in native A and B, respectively. The Ca^{2+} concentrations in the buffers are 10 to 30 μM.
13. In native A, the *B* factor for a K^+ ion at site 1 refined with full occupancy is 13 $Å^2$, compared with an average ligand value of 19 $Å^2$. Refinement of Na^+, or Ca^{2+} with partial occupancy, results in very low metal *B* factors and strong, positive difference electron density centered on the metal ion. Refinement of K^+ with full occupancy at site 2 in native A gives a *B* factor (47 $Å^2$) that is significantly higher than the average ligand value (19 $Å^2$). In contrast, Na^+ with full occupancy at site 2 yields a *B* factor of 26 $Å^2$ compared with an average ligand value of 19 $Å^2$. In native B, Na^+ refined with full occupancy at site 1 has a *B* factor of 31 $Å^2$ compared with an average ligand value of 24 $Å^2$. At site 2, Na^+ refined with full occupancy has a *B* factor of 31 $Å^2$ compared with an average ligand value of 27 $Å^2$. Refinement of several alternative native B models with partial occupancies for K^+ or Ca^{2+} invariably yielded either *B* factors significantly different from the average ligand values or strong residual difference density centered on the metal ion, or both.
14. Standard metal-oxygen distances are 2.1 Å for Mg^{2+}, 2.4 Å for Na^+ and Ca^{2+}, and 2.7 to 2.8 Å for K^+ [J. P. Glusker, *Adv. Protein Chem.* **42**, 1 (1991); C. A. McPhalen, N. C. J. Strydnadka, M. N. G. James, *ibid.*, p. 77; M. M. Yamashita, L. Wesson, G. Eisenman, D. Eisenberg, *Proc. Natl. Acad. Sci. U.S.A.* **87**, 5648 (1990)]. The average metal-ligand distances obtained for the metals assigned to the final models are 2.73 and 2.33 Å at site 1 and 2.39 and 2.42 Å at site 2 in native A and native B, respectively. Metal-ligand distances were completely unrestrained during the refinement procedures, and no electrostatic or van der Waals energy terms were used.
15. DGD requires K^+ ions for activity and stability, whereas Li^+ and Na^+ are inhibitory [H. G. Aaslestad, P. J. Bouis, Jr., A. T. Philips, A. D. Larson, in *Pyridoxal Catalysis: Enzymes and Model Systems*, E. E. Snell, A. E. Braunstein, E. S. Severin, Y. M. Torchinsky, Eds. (Wiley-Interscience, New York, 1968), pp. 479–490].
16. G. Eisenman and J. A. Dani, *Annu. Rev. Biophys. Biophys. Chem.* **16**, 205 (1987); M. Dobler, *Ionophores and Their Structures* (Wiley, New York, 1981); R. M. Izatt *et al.*, *Chem. Rev.* **85**, 271 (1985); F. Vögtle and E. Weber, Eds., *Host Guest Complex Chemistry: Macrocycles* (Springer, Berlin, 1985); D. Cram, *Angew. Chem. Int. Ed. Engl.* **25**, 1039 (1986).
17. C. H. Suelter, *Science* **168**, 789 (1970). Nonspecific binding of Na^+ and K^+ ions to proteins has been observed crystallographically with subtilisin BPN′ [M. W. Pantoliano *et al.*, *Biochemistry* **27**, 8311 (1988)], thermitase [P. Gros *et al.*, *J. Mol. Biol.* **210**, 347 (1989)], and insulin [O. Gursky, Y. Li, J. Badger, D. L. D. Caspar, *Biophys. J.* **61**, 604 (1992)]. Crystallographic observation of the essential K^+ ion in pyruvate kinase has remained elusive [H. Muirhead, in *Biological Macromolecules and Assemblies*, F. A. Jurnak and A. McPherson, Eds. (Wiley-Interscience, New York, 1987), vol. 3, pp. 143–186].
18. M. Carson, *J. Mol. Graph.* **5**, 103 (1987).
19. We thank J. W. Keller for supplying the enzyme, P. Maurer for performing the calcium determination experiments, and U. Sauder for providing expert technical assistance. Supported by Swiss National Science Foundation grant 31-25712.88 (J.N.J.) and by U.S. National Institutes of Health fellowship GM13854 (M.D.T.).

16 March 1993; accepted 25 June 1993

DNA Melting on Yeast RNA Polymerase II Promoters

Charles Giardina and John T. Lis*

Transcription-dependent DNA melting on the yeast *GAL1* and *GAL10* promoters was found to be more closely correlated with the TATA box than the transcription start site. On both these genes, melting begins about 20 base pairs downstream of the TATA box. Physical and genetic analyses suggest that RNA polymerase II associates with this region. Thus, the distance between promoter melting and the TATA box in yeast may be similar to that in higher eukaryotes, even though transcription initiates in a region about 10 to 90 base pairs farther downstream in yeast.

In prokaryotes, the melting of the DNA helix at the commencement of transcription often requires only the RNA polymerase and promoter sequence elements (*1*). For eukaryotic RNA polymerase II genes, this melting reaction also depends on RNA polymerase II but in addition requires basal transcription factors and adenosine triphosphate (ATP) hydrolysis (*2*). On TATA-containing promoters, the transcription factor TFIID first associates with the TATA box followed by the other basal factors and polymerase (*3*). After this assembly, the DNA can be melted in an ATP-dependent reaction, with residues approximately 12 base pairs (bp) upstream through 3 bp downstream of the transcriptional start site being unwound to form an open complex (*4*, *5*).

In higher eukaryotes, the locations of promoter melting and transcription initiation overlap at ~30 bp from the TATA box (*4–6*). In yeast the distance between the location of the transcriptional startsite and the TATA box is highly variable, ranging from 30 to 120 bp (*7*). This is true even though the basal transcription factors and the polymerase are highly conserved between yeast and higher eukaryotes (*8–12*). We wanted to determine, therefore, how promoter melting in yeast is positioned relative to the start site and the TATA box. We used the DNA modifying reagent potassium permanganate ($KMnO_4$) which reacts preferentially with T residues in single-stranded DNA (*13*). Although open polymerase complexes can be difficult to detect under steady-state conditions, $KMnO_4$ hyperreactivity of these complexes can be detected on some promoters in *Escherichia coli* (*14*). We have also detected what appear to be open polymerase complexes in *Drosophila* cells in vivo, suggesting that these complexes have a dwell time long enough to allow their detection in eukaryotes (*15*).

Section of Biochemistry, Molecular, and Cell Biology, Cornell University, Ithaca, NY 14853.

*To whom correspondence should be addressed.